Incomplete vesicular docking limits synaptic strength under high release probability conditions

Gerardo Malagon[1,2], Takafumi Miki[1,3], Van Tran[1], Laura C Gomez[1], Alain Marty[1]*

[1]Université de Paris, SPPIN-Saints Pères Paris Institute for the Neurosciences, CNRS, Paris, France; [2]Department of Cell Biology and Physiology, Washington University, St. Louis, United States; [3]Graduate School of Brain Science, Doshisha University, Kyoto, Japan

Abstract Central mammalian synapses release synaptic vesicles in dedicated structures called docking/release sites. It has been assumed that when voltage-dependent calcium entry is sufficiently large, synaptic output attains a maximum value of one synaptic vesicle per action potential and per site. Here we use deconvolution to count synaptic vesicle output at single sites (mean site number per synapse: 3.6). When increasing calcium entry with tetraethylammonium in 1.5 mM external calcium concentration, we find that synaptic output saturates at 0.22 vesicle per site, not at 1 vesicle per site. Fitting the results with current models of calcium-dependent exocytosis indicates that the 0.22 vesicle limit reflects the probability of docking sites to be occupied by synaptic vesicles at rest, as only docked vesicles can be released. With 3 mM external calcium, the maximum output per site increases to 0.47, indicating an increase in docking site occupancy as a function of external calcium concentration.

Introduction

The release of synaptic vesicles (SVs) at mammalian central synapses is a complex process that comprises two series of events. Firstly, SVs move to a small part of the presynaptic terminal, the active zone (AZ), where they bind to specific proteins such as RIM and Munc13, and undergo a number of maturation steps including docking and priming (*Südhof, 2012*; *Jahn and Fasshauer, 2012*). At the end of these preparatory processes, SVs are connected to the plasma membrane through SNARE complexes, and they are ready for exocytosis. Secondly, mature SVs fuse with the plasma membrane following a rapid increase in local Ca^{2+} concentration (Ca_i), leading to the release of neurotransmitter. The sensitivity of the exocytosis step to Ca_i results from the change of conformation of the SNARE complex following rapid Ca^{2+} binding to a series of Ca^{2+} binding sites residing on synaptotagmins (*Jahn and Fasshauer, 2012*). Experiments combining Ca^{2+} uncaging and Ca_i measurement in presynaptic terminals with postsynaptic EPSC recording have demonstrated that these sites have a low affinity for Ca^{2+} and fast kinetics (*Bollmann et al., 2000*; *Schneggenburger and Neher, 2000*). The corresponding Ca^{2+}-dependent reactions generate a characteristic curve describing the rate of SV exocytosis as a function of Ca_i. At low Ca_i values, the response follows a sigmoid rise with a Hill coefficient close to 4. At high Ca_i values, the response saturates, presumably because all available SVs undergo exocytosis. Based on these findings, various multistep kinetic models of SV release have been proposed, where the probability of exocytosis reaches a maximum of 1 for high Ca_i values (*Bollmann et al., 2000*; *Schneggenburger and Neher, 2000*; *Lou et al., 2005*).

The docking/priming steps preceding exocytosis have been extensively studied in recent years. TIRF results using single SV tracking in calyx of Held terminals indicate a sequence of a long-lived (about 3 s long) tethered state (at a distance of <100 nm from the plasma membrane), followed by

shorter-lived (about 0.3 s long) docked, and docked/primed states, before exocytosis (*Midorikawa and Sakaba, 2015*). These results indicate that certain docking/priming steps are much slower than exocytosis. However other results using electrophysiological recordings indicate that in some preparations, the last preparatory step before exocytosis can occur within a few ms only (*Saviane and Silver, 2006*; *Hallermann et al., 2010*; *Miki et al., 2016*; *Kawaguchi and Sakaba, 2017*; *Miki et al., 2018*). In agreement with these studies, a recent electron microscopy study of synaptotagmin-1 modified mouse mutants demonstrates that in these mouse lines, docking of synaptic vesicles occurs within 10 ms following action potential stimulation (*Chang et al., 2018*). Another electron microscopy study carried out on wild type animals showed that following a presynaptic action potential, complex undocking/docking sequences occur on a time scale ranging from 5 to 100 ms (*Kusick et al., 2018*). These results indicate that the last step before exocytosis involves a fast, Ca^{2+}-dependent SV movement towards the plasma membrane, and they suggest some degree of integration between preparatory steps and exocytosis (*Neher and Brose, 2018*).

Recently our group has developed methods to investigate SV release in 'simple synapses', small central synapses that contain a single presynaptic active zone (review: *Pulido and Marty, 2017*). Simple synapse recording in cerebellar slices has provided precise information on SV release and has led to several observations indicating that docking sites are not fully occupied at rest, both in GABAergic connections between molecular layer interneurons (MLIs), and in glutamatergic connections between parallel fibers (PFs) and MLIs: (i) in MLI-MLI simple synapses, responses to repeated saturating Ca^{2+} uncaging stimulations display trial to trial fluctuations (*Trigo et al., 2012*); (ii) when testing the responses of simple MLI-MLI synapses to presynaptic action potentials, individual docking sites fluctuate between periods of low release probability and periods of high release probability (*Pulido et al., 2015*); (iii) synaptic facilitation at simple PF-MLI synapses is most simply explained by assuming partial resting docking site occupancy (*Miki et al., 2016*). In spite of these various lines of evidence, however, present estimates for the probability of docking site occupation remain tentative, because of the difficulty in separating this probability from the release probablilty of occupied sites.

Model simulations indicate that the docking site occupancy at rest strongly influences short-term synaptic plasticity and statistics of SV release (*Pulido and Marty, 2018*; *Miki, 2019*). In addition, the proposal of partial docking site occupancy at rest has important implications concerning the maximum response of a synapse. Because a release site needs a docked SV to release, partially occupied docking sites should display a release probability following AP stimulation that remains below 1, even if experimental conditions are chosen to maximize release of docked SVs. To test this prediction, we explore in the present work how high release conditions alter the behavior of simple synapses. We estimate release site numbers in each recording, and obtain absolute numbers for the release probability per release site. We then produce dose-response curves by combining these results with measurements of calcium entry in single varicosities. Comparing the dose-response curve with the predictions of current models of Ca^{2+}-dependent exocytosis confirms the notion that docking site occupancy is incomplete at rest, and that partial site occupancy limits the synapse output at high release probability. Furthermore, our results suggest that docking site occupancy grows as a function of the external Ca^{2+} concentration, $[Ca^{2+}]_o$. They further suggest that a given $[Ca^{2+}]_o$, the docking site occupancy can be obtained as the maximal attainable release probability per release site. Finally, our results suggest that previous apparently discrepant results indicating a very high (close to 1) maximal release probability per release site can be explained partially by uncorrected errors in variance-mean analysis, and partially by changes of docking site occupancy with $[Ca^{2+}]_o$.

Results

Release probability per docking site during AP trains

In this work we examine counts of SV release events measured in simple PF-MLI synapses when increasing the release probability with several methods. Our aim is to identify the source(s) of the increase of release probability in each case, taking advantage of the detailed information provided by SV counting in individual AZs. As further discussed below, we assume for the interpretation of our results that release occurs at a finite set of docking/release sites, and that SVs undergo

exocytosis only once they are docked. Within this simple docking/release model, we attempt to distinguish increased probability of docking site occupancy by SVs from increased probability of exocytosis of an occupied docking site (*Quastel, 1997*).

Figure 1A illustrates the experimental protocol. Having established a recording in an MLI, a pipette was placed either in the granule cell layer or in the molecular layer to stimulate extracellularly a presynaptic granule cell or its associated PF axon. The pipette position and stimulation strength were carefully adjusted to restrict the stimulation to a single presynaptic PF (see Materials and methods; *Malagon et al., 2016*; *Miki et al., 2017*). Trains of 8 action potentials (APs) were applied at a frequency of 100 Hz inside a train, leaving 10 s intervals between trains. Typical traces in response to an 8-AP stimulation train (stimulation times: vertical red bars) are shown in *Figure 1A*. As illustrated in this example, responses to individual APs varied between single quantal responses (with unitary amplitudes on the order of 100 pA or more in this preparation: *Llano and Gerschenfeld, 1993*; examples in responses to 1 st and 2nd AP in 1 st trace), failures (as following 3rd and 4th AP of 1 st trace), and multivesicular responses (eg, following the 5th stimulation in the 1 st trace). Only results passing previously defined criteria for simple synapse recordings were accepted in this work (*Malagon et al., 2016*). Briefly, the criteria were: (i) stability of the recording as a function of time; (ii) amplitude occlusion for consecutive events at short intervals; (iii) low scatter of quantal current amplitudes (*Malagon et al., 2016*). In recordings that met these criteria, we identified single release events during AP trains by deconvolution, using a synapse-specific averaged quantal EPSC profile as template (*Malagon et al., 2016*). We then summed the numbers of SVs released in a 5 ms long time window following each AP stimulation. These numbers represent the output of individual AZs following AP stimulations. They are depicted in matrices as a function of AP number and train number in *Figure 1B*, where grey levels represent various SV numbers.

A first set of experiments was performed under normal release conditions, using an external Ca^{2+} concentration ($[Ca^{2+}]_o$) of 1.5 mM. We then observed a gradual increase in SV counts during a train, reflecting facilitation (*Figure 1B*, upper panel; group data in *Figure 1D*, pink). After obtaining a series of train responses, SV counts were calculated separately for each of the 8 successive AP stimulations, and we calculated means and variances of SV counts according to the AP stimulation number, i. This gave a variance vs. mean plot with 8 data points that could be fitted using a parabola (*Figure 1C*). To interpret these data we assumed that each simple synapse obeys a binomial release process, with N functional units (docking/release sites) acting in parallel (*Malagon et al., 2016*). The intersect of the parabola with the abscissa axis yielded the value of N. For stimulus number i, we calculated the probability P_i that a docking site releases a SV by dividing the mean SV count by N, with a mean N value of 3.6 across synapses. The mean of P_1 obtained in this manner under control conditions was 0.089 ± 0.015 while the mean of the maximum of P_i for i = 1–8 was P_{max} = 0.270 ± 0.027. These data show that facilitation markedly increases P under control conditions, with a ratio between P_1 and P_{max} of 3-fold. They also indicate that P is far from reaching the maximum value of 1 under these conditions.

Effect of adding 1 mM TEA on P

Standard docking/release site models assume that a docking site can release only if it is occupied by a SV. Accordingly, these models predict that P_i is the product of δ_i and p_i, where δ_i is the mean docking site occupancy (sometimes noted p_{occ}) before stimulus number i, and p_i is the probability of release of a docked SV (sometimes noted p_{ves}) following stimulus number i (*Vere-Jones, 1966*; *Zucker, 1973*; *Quastel, 1997*; *Scheuss and Neher, 2001*). In the following we will accept the $P_i = \delta_i p_i$ relation as a guideline. Recent results calling for a qualification of this hypothesis (*Miki et al., 2018*) will be discussed below.

Increasing evidence indicates that both facilitation and depression mostly follow changes in docking site occupancy, reflecting a trade-off between SV loss by exocytosis and SV gain by docking site replenishment (*Pulido et al., 2015*; *Miki et al., 2016*; *Miki et al., 2018*). Accordingly, we assume in the following that p_i takes a common value, p, independently of i, so that $P_i = \delta_i p$. For i = 1 we write $\delta_1 = \delta$, and $P_1 = \delta p$, where δ is the resting docking site occupancy. In line with our previous work (*Miki et al., 2016*; *Miki et al., 2017*), we further assume that all release sites have the same release probability and that they are located at equal distances from presynaptic voltage-dependent calcium channels.
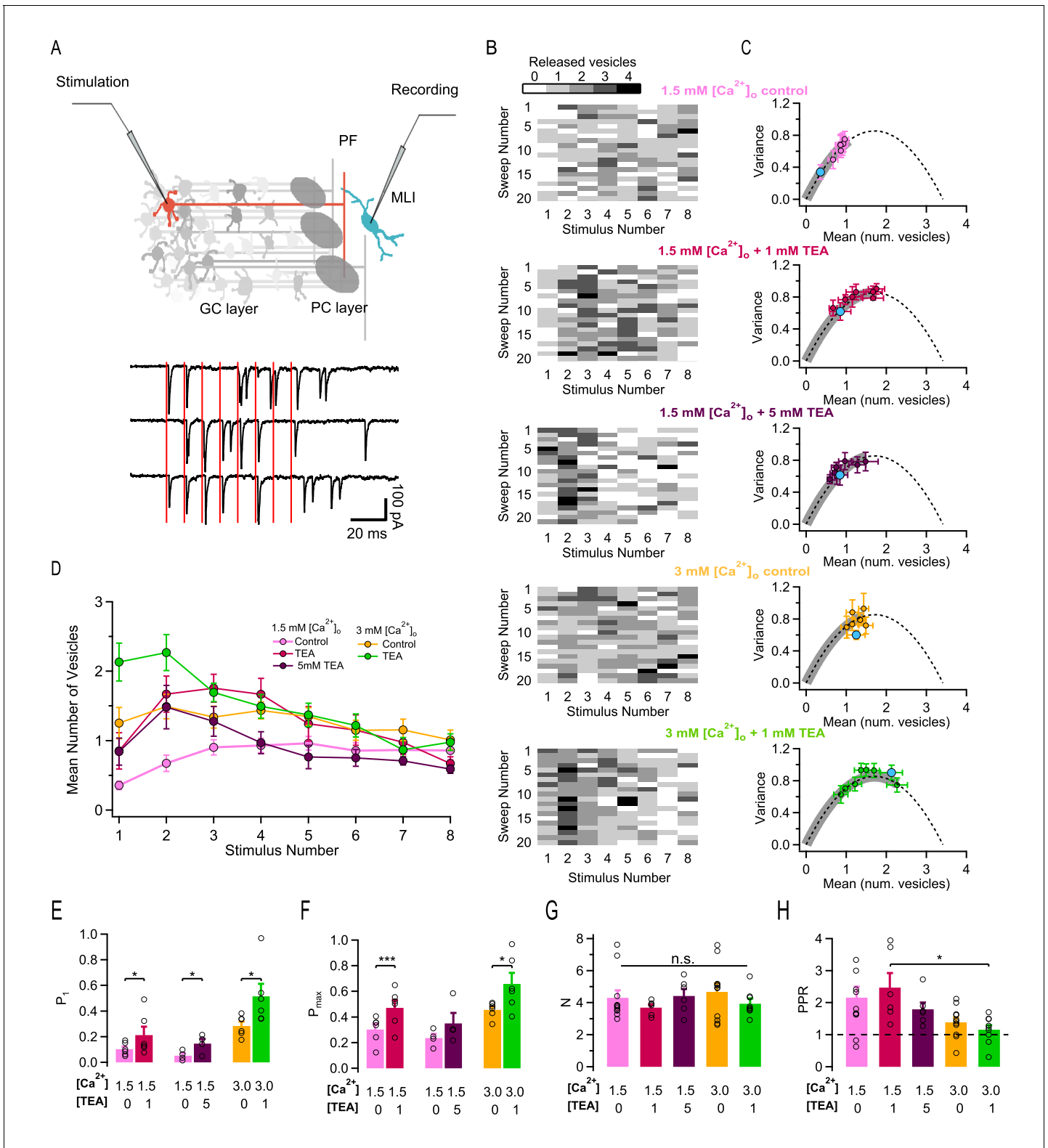
Figure 1. Effects of different release conditions on synaptic parameters and short-term plasticity. (**A**) Upper panel: Schematics of recording configuration. A stimulation pipette is positioned close to the soma of a potential presynaptic granule cell while whole-cell recording from a MLI. Careful presynaptic pipette positioning and stimulation strength adjustment results in selective stimulation of a single PF-MLI connection. Lower panel: Individual traces in response to AP trains (8 stimuli, 100 Hz; stimulation timing in red). (**B**) Deconvolution-based counts of released SVs per stimulus. Matrices of SV numbers as a function of AP number for 5 individual experiments are illustrated in different external solutions (from top to bottom: 1.5

Figure 1 continued on next page

Figure 1 continued

mM $[Ca^{2+}]_o$ in control, in 1 mM TEA, and in 5 mM TEA; 3 mM $[Ca^{2+}]_o$ in control and in 1 mM TEA). Each experiment involved a control period and another set of data in one TEA concentration. Accordingly, the two SV count matrices in 1.5 mM $[Ca^{2+}]_o$ without TEA and with 1 mM TEA stem from the same experiment. Likewise, the two SV count matrices in 3 mM $[Ca^{2+}]_o$ without TEA and with 1 mM TEA stem from the same experiment. (C) Group results of the variance-mean relationship of the number of released vesicles calculated per stimulus (mean ± SEM; results for the first stimulus in blue). The dashed lines represent the parabolic fit after pooling the results in all conditions; it indicates an N = 3.6. Gray thick traces show the excursion over this parabola from the origin until the value that displays the highest P. (D) Time course of SV numbers during a train showing changes in short term synaptic plasticity with $[Ca^{2+}]_o$ and TEA (same data set as in C). (E–H) Group analysis (bars: mean ± SEM, n = 4–12; circles: individual experiments) show an increase of the release probability for the 1st stimulus as a function of TEA (E), an increase of the maximal release probability as a function of TEA (F), no change in N (G), and a decrease of the PPR as a function of $[Ca^{2+}]_o$ and TEA (H). Statistical comparisons use paired t-tests in E-F, and unpaired t-tests for all combinations in G-H. No symbol or n.s. = $p > 0.05$; *=$p < 0.05$; **=$p < 0.01$; ***=$p < 0.001$.

The online version of this article includes the following figure supplement(s) for figure 1:

Figure supplement 1. Effect of adding TEA on granule cell excitability.

While the value of P_1 is readily accessible by performing variance-mean analysis of SV counts, as explained above, separating p from δ poses a challenge. An attractive way to determine δ is to increase the amount of Ca^{2+} entry until p reaches one because in this case, the relation $P_1 = δ p$ becomes $P_1 = δ$. Therefore, measuring P_1 under very high release probability conditions provides a direct estimate of δ.

We therefore explored ways to increase p in the present work. Previous studies indicate that addition of TEA increases p in many synapses including PF-MLI synapses by broadening AP duration and increasing the amount of Ca^{2+} entry per AP, mainly by blocking Kv3 channels (*Sabatini and Regehr, 1997*; *Ishikawa et al., 2003*). When applying TEA in granule cell recordings, we found in agreement with previous work (*Sabatini and Regehr, 1997*) a decrease in voltage-dependent K^+ current amplitudes and an increase in AP duration (*Figure 1—figure supplement 1*). Furthermore, TEA increased the responses of PF-MLI synapses to AP stimulations (*Figure 1B*: compare first and second panel from above). Comparing released SV counts before and after the addition of TEA in the same experiment, as illustrated in the example of *Figure 1B*, shows a marked increase in the presence of TEA. Average SV counts across experiments for the first AP were $n_1 = 0.36 ± 0.06$ in control and $n_1 = 0.85 ± 0.26$ in TEA (n = 6; p<0.05, paired t-test). Variance-mean analysis of SV counts (*Figure 1C*, first and second graphs from top) showed no change of N upon application of TEA (individual experiments and corresponding means in *Figure 1G*). Given that N stays constant, the change in synaptic strength associated with TEA application is entirely mediated by an increase in P. After normalizing SV counts per docking site, we found that P_1 values increased from 0.103 to 0.213 in 1 mM TEA (*Figure 1E*).

Despite this marked increase in P_1, the responses to an 8-AP train displayed roughly the same amount of facilitation with and without TEA. Paired-pulse ratio (PPR) values, obtained by calculating the ratio of n_2/n_1, were similar with and without TEA (two first columns in *Figure 1H*). When examining the time course of n_i values during the train, the maximum P_{max} was attained earlier in TEA (for i = 3) than in control (for i = 5), but the shapes of the two curves were not strikingly different (compare pink and red curves in *Figure 1D*). These observations are in line with the fact that the value of P_1 obtained in TEA (0.213) is far from the maximum attainable value of 1, leaving room for a significant increase of P linked to facilitation.

Finally, the value of P_{max} in the presence of 1 mM TEA was 0.472, far below the maximum of 1. Therefore, increasing release probability by a combination of synaptic facilitation and of TEA application is not sufficient to bring the release probability to 1.

Saturation of P as a function of TEA concentration

A possible interpretation of the results above is that addition of 1 mM TEA was insufficient to bring the release probability of a docked SV (p) to its maximum of 1. To investigate this possibility, we tested 5 mM TEA in a new series of experiments, starting again from the same 1.5 mM $[Ca^{2+}]_o$ control condition (*Figure 1B*, third row). As documented below, Ca^{2+} entry was substantially increased in 5 mM TEA compared to 1 mM TEA. Nevertheless, even with 5 mM TEA, failures were often observed in response to the 1 st AP (*Figure 1B*, third row), suggesting that P_1, the probability that a site releases a SV after the 1st AP, was still far from reaching its maximum of 1. In these experiments,

P_1 grew from 0.053 ± 0.018 without TEA to 0.146 ± 0.036 in 5 mM TEA. This represented a mean P_1 ratio of 3.0 in individual experiments, not significantly different from the 1.9-fold ratio obtained in the previous experiments with 1 mM TEA (unpaired t-test). Globally these results suggest that TEA increases P_1 only up to a certain point.

If p is close to 1 in both 1 mM and 5 mM TEA, then in view of the relation $P_1 = p \delta$, P_1 is close to δ in both cases. Therefore, an obvious possible explanation for the limitation of P_1 near 0.2 is that this limit represents δ, the docking site occupancy. Starting with a common submaximal δ value leaves the same room for δ-driven facilitation in 1 mM TEA experiments and in 5 mM TEA experiments. In line with this suggestion, we found similar values for the PPR (2.47 ± 0.45 in 1 mM TEA vs. 1.80 ± 0.21 in 5 mM TEA; n. s.) and for P_{max} (0.472 ± 0.059 in 1 mM TEA vs. 0.351 ± 0.080 in 5 mM TEA; n. s.) in 1 mM TEA and in 5 mM TEA.

In summary, values of P_1, P_{max} and PPR are similar in 1 mM TEA and in 5 mM TEA, suggesting saturation of p as a function of TEA concentration. In 5 mM TEA as in 1 mM TEA, the variance-mean curve remains restricted to the ascending limb of the parabola, where the release probability is less than 0.5 (grey thick lines in *Figure 1C*, 2nd and 3rd panels from above).

Release statistics as a function of extracellular Ca^{2+} concentration

In view of our failure to reach $P = 1$ by addition of TEA, we next studied SV release in elevated (3 mM) $[Ca^{2+}]_o$ conditions, both with and without TEA, and we compared the results with those previously obtained under control $[Ca^{2+}]_o$ (1.5 mM).

We first examined results in 3 mM $[Ca^{2+}]_o$ without TEA. In 3 mM $[Ca^{2+}]_o$, P_1 was increased compared to 1.5 mM $[Ca^{2+}]_o$ (0.28 ± 0.03 vs. 0.089 ± 0.015; $p<0.01$, unpaired t-test), and it reached a mean value similar to that obtained in 1.5 mM $[Ca^{2+}]_o$ and TEA (0.28 ± 0.03 vs. 0.21 ± 0.06). Likewise P_{max} was larger in 3 mM $[Ca^{2+}]_o$ compared to 1.5 mM $[Ca^{2+}]_o$ (0.46 ± 0.04 vs. 0.27 ± 0.03; $p<0.01$, unpaired t-test), and was similar in 3 mM $[Ca^{2+}]_o$ compared to 1.5 mM $[Ca^{2+}]_o$ and TEA (0.46 ± 0.04 vs. 0.47 ± 0.06).

The finding that P_1 and P_{max} take similar values in 3 mM $[Ca^{2+}]_o$ and in 1.5 mM $[Ca^{2+}]_o$ plus TEA could reflect a common limit to the strength of the synapse. Alternatively, it could be a sheer numerical coincidence. To distinguish between these two possibilities, we next tested the effects of adding 1 mM TEA starting in 3 mM $[Ca^{2+}]_o$. P_1 significantly increased from 0.28 ± 0.03 to 0.51 ± 0.09 ($p<0.05$, paired t-test; exemplar experiment in lowest 2 panels of *Figure 1B*; group results in *Figure 1E*). Likewise, P_{max} increased from 0.46 ± 0.04 to 0.66 ± 0.08 ($p<0.05$, paired t-test; *Figure 1F*). Therefore, whereas neither P_1 nor P_{max} increased significantly when increasing the TEA concentration from 1 to 5 mM in 1.5 mM $[Ca^{2+}]_o$ experiments, both P_1 and P_{max} were significantly higher in 3 mM $[Ca^{2+}]_o$ and 1 mM TEA compared to 3 mM $[Ca^{2+}]_o$. These results indicate that combining $[Ca^{2+}]_o$ elevation with TEA application is an effective way to overcome the limitations in P apparent at high TEA concentrations with normal $[Ca^{2+}]_o$.

TEA and $[Ca^{2+}]_o$ increase P by two different mechanisms

In view of the relation $P = \delta p$, we propose as an interpretation of the above results that TEA application leads to an increase of p without a change in δ, whereas an increase in $[Ca^{2+}]_o$ results in increases in both δ and p. In this interpretation, δ remains constant if $[Ca^{2+}]_o$ is constant, so that even if TEA increases p near its maximum $p = 1$, P remains limited by δ. This explains the limitation of P_1 values near 0.2 in 1.5 mM $[Ca^{2+}]_o$ (*Figure 1E*). By contrast if $[Ca^{2+}]_o$ is increased the value of δ increases so that the maximum attainable for P_1 increases according to the change in δ. This explains the higher P_1 values observed when combining TEA and high $[Ca^{2+}]_o$, compared to applying TEA in normal $[Ca^{2+}]_o$ (*Figure 1E–F*).

The proposal of differential effects of TEA and $[Ca^{2+}]_o$ on p and δ also helps explaining short-term plasticity results shown in *Figure 1*. As detailed earlier (*Pulido and Marty, 2018*), models of synaptic function based on changes in docking site occupancy predict different effects of increasing p or δ on short-term synaptic plasticity. While all synapses become depressing if δ increases to the maximum $\delta = 1$, some synapses with low δ values remain facilitating even if p increases to $p = 1$. This is because if the initial value of docking site occupancy is low, even if the first AP releases all docked SVs, replenishment of initially empty docking sites can overcompensate the loss of exocytosed SVs, resulting in facilitation. In the present case, while facilitation was prominent in 1.5 mM

$[Ca^{2+}]_o$, without and with TEA, it became weak or absent in 3 mM $[Ca^{2+}]_o$ (yellow and green curves in *Figure 1D*). Simultaneously depression increased, particularly in the presence of TEA (green curve in *Figure 1D*), and the value of the PPR decreased (*Figure 1H*). Overall, the finding that facilitation remains when applying TEA alone is consistent with a pure effect on p, while the more complex effects observed on short-term synaptic plasticity when increasing $[Ca^{2+}]_o$ are consistent with a mixed effect on p and δ.

Miniature current frequencies in elevated $[Ca^{2+}]_o$ and in TEA

In several synapses including MLI synapses onto Purkinje cells, increasing $[Ca^{2+}]_o$ leads to an increase of miniature current frequency, presumably following an increase in the presynaptic resting $[Ca^{2+}]_i$ (*Llano et al., 2000*). At PF-MLI synapses, we found that miniature EPSC frequency rose from 0.142 ± 0.033 Hz in 1.5 mM $[Ca^{2+}]_o$ to 0.364 ± 0.040 Hz in 3 mM $[Ca^{2+}]_o$ (p<0.01; n = 6), while mean peak miniature EPSC amplitudes did not change significantly (93.6 ± 9.1 pA in 1.5 mM $[Ca^{2+}]_o$ vs. 105.3 ± 20.4 pA in 3 mM $[Ca^{2+}]_o$; p>0.05; n = 6). These data suggest that elevating $[Ca^{2+}]_o$ results in an elevation of presynaptic $[Ca^{2+}]_i$ at PF-MLI synapses. By contrast, we found that TEA (1 mM) did not change miniature EPSC frequency (control frequency: 0.123 ± 0.014 Hz; TEA frequency: 0.116 ± 0.023 Hz, p>0.05, n = 7). These results suggest that $[Ca^{2+}]_o$ elevation, but not TEA addition, leads to an increase in the presynaptic basal $[Ca^{2+}]_i$. As SV replenishment is enhanced by elevations of $[Ca^{2+}]_i$ (*Neher and Sakaba, 2008*), it is plausible that presynaptic $[Ca^{2+}]_i$ elevation increases the docking site occupancy δ.

Comparison of variance-mean analyses performed on SV counts and on EPSC peak amplitudes

A striking outcome of the experiments described so far is that in all cases, variance-mean parabolas were far from complete, as illustrated by the thick grey curves in *Figure 1C*. Specifically, in spite of our efforts, we were unable to attain a value of P larger than 0.66 in the above experiments (i. e., the value of P_{max} in 3 mM $[Ca^{2+}]_o$ and 1 mM TEA). This contrasts with many studies reporting P values of 0.9 or larger when performing mean-variance analysis of peak EPSC amplitudes (*Branco and Staras, 2009*). One possible reason for the discrepancy is that P is limited by δ, as mentioned above, and that the value of δ is particularly low in PF-MLI synapses. Another possible reason is methodological. In the traditional method of peak EPSC mean-variance analysis, receptor saturation or desensitization, as well as synaptic jitter, can lead to substantial errors (*Clements, 2003*; *Silver, 2003*). These errors worsen at high release probability, and if they are not corrected, their effects tend to overestimate P and to underestimate N. While methods exist to correct for some of these errors (*Silver, 2003*; *Taschenberger et al., 2005*), corrections are difficult to implement, often requiring dedicated experiments, and they are at best partial. To examine the potential consequences of the errors involved, we next compared in the same recordings the P value obtained from peak EPSC analysis with the value obtained from SV counts.

A comparison between the two kinds of variance-mean analyses is presented in *Figure 2A* in an experiment using 3 mM $[Ca^{2+}]_o$. The variance-mean parabola indicated a P_1 value of 0.307 with the SV count method (left, red triangles) and of 0.487 with the peak EPSC method (center, open purple rectangles); P_{max} values were 0.436 with the SV count method and 0.710 with the peak EPSC method. As illustrated in this example, P estimates were invariably higher with the EPSC amplitude analysis than with the SV count analysis. The discrepancy became larger when correcting the variance for EPSC amplitudes for the variations in q values in the same experiment (filled purple rectangles, right panel: $P_1 = 0.530$, and $P_{max} = 0.779$), as is usually done in peak amplitude variance-mean analysis (*Silver, 2003*). To perform the correction, we assumed a CV value of 0.30 for quantal amplitude variance within one synapse, based on previous estimates (*Malagon et al., 2016*). Average results revealed significant discrepancies in P_1 estimates in 3 mM $[Ca^{2+}]_o$ (0.294 ± 0.032 with the SV count method vs. 0.612 ± 0.058 with the peak EPSC method, p<0.001; *Figure 2B*; note that the present values obtained with the peak EPSC method are in agreement with previous estimates in the same preparation using the same method: *Ishiyama et al., 2014*). Similarly, P_{max} estimates were smaller with the SV count method than with the peak EPSC method (0.456 ± 0.025 vs. 0.806 ± 0.058, p<0.01; *Figure 2C*). Estimated N values were larger with the SV counting method than with the peak EPSC method (3.94 ± 0.46 vs. 2.19 ± 0.29, p<0.05; *Figure 2D*), suggesting that the peak EPSC
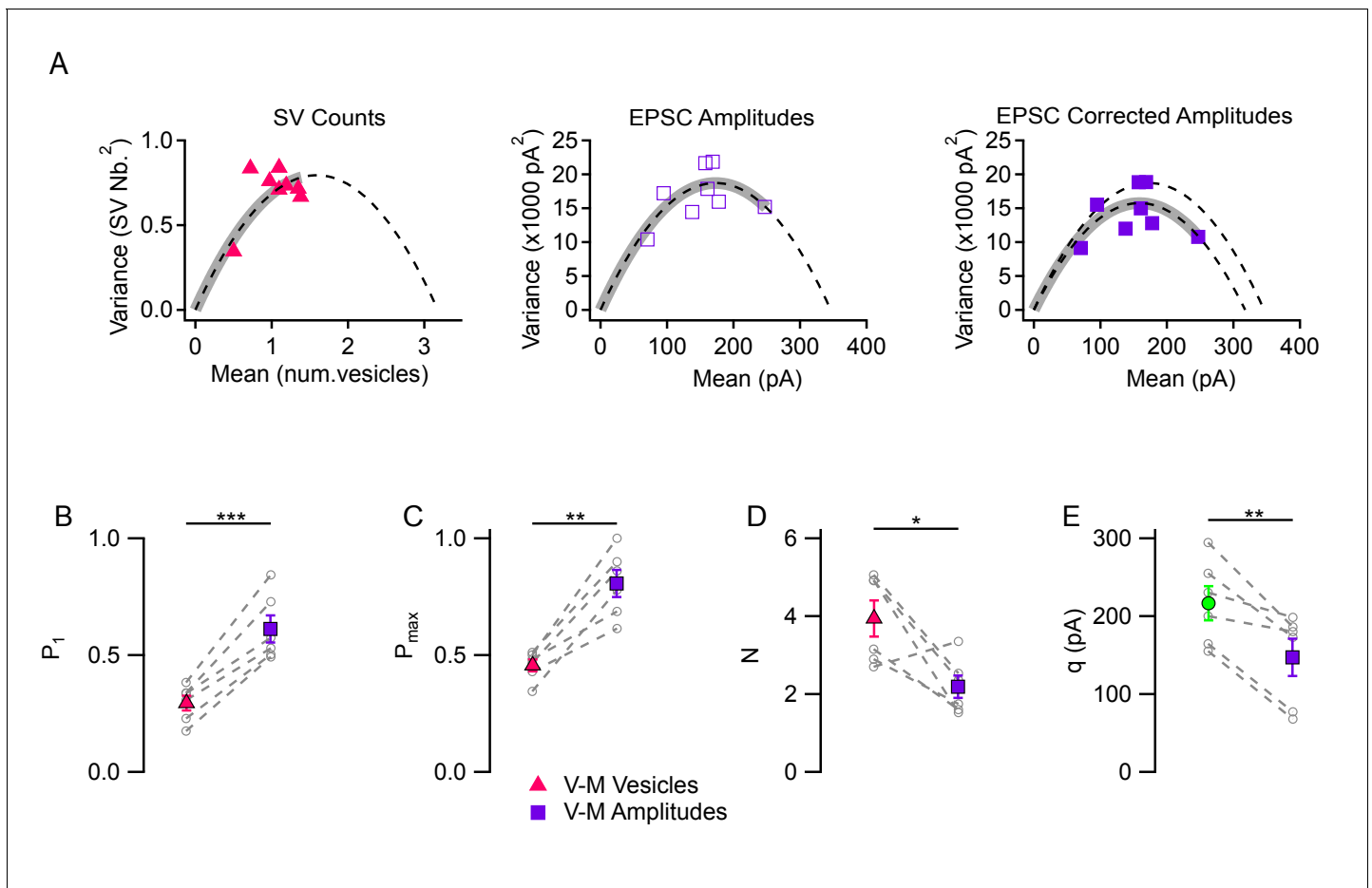
Figure 2. Comparison between variance-mean analysis of SV counts and variance-mean analysis of peak EPSC amplitudes. (**A**) Variance vs. mean plots calculated for different stimulus numbers (8 stimuli per plot) in a representative simple synapse experiment (3 mM $[Ca^{2+}]_o$). Using the same data, mean and variance estimates were obtained either using SV counts (left, triangles) or using peak EPSC amplitudes (center and right, squares). Fitted functions follow the equations $f(x)=x - x^2/N$ for SV counts, and $f(x)=x \, q – x^2/N$ for EPSC amplitudes (dashed lines: parabolic fits; gray thick traces show the excursion over the parabola from the origin up to the experimental point with highest P value). The right panel shows the effect of correcting the variance in the peak EPSC analysis for variations in q size ('corrected amplitudes': filled squares). The thick grey parabolas indicate a larger maximum P value with EPSC amplitude analysis than with SV counts, particularly after correction. (**B–D**) Group analysis of synaptic parameters extracted from 6 experiments as illustrated in (**A**) using variance-mean analysis based either on SV counts (triangles) or EPSC amplitudes (filled squares; data corrected for q variance). These results show higher estimates of P_1 and P_{max}, as well as lower N estimates, when using EPSC amplitudes compared to using SV counts. (**E**) Quantal size estimates using variance-mean analysis of EPSC amplitudes (mean: purple square) are lower than direct measurements obtained for each synapse during delayed release (mean: green circle). In (**B–E**), error bars show ± SEM, and results from same experiments are linked together with dashed lines. Statistical comparisons show results of paired t-tests between indicated data groups: *=$p < 0.05$; **=$p < 0.01$; ***=$p < 0.001$.

method leads to an underestimate of N. Finally, direct measurements of quantal current amplitudes (217 ± 22 pA) were significantly different from q estimates derived from EPSC amplitude variance-mean analysis (147 ± 24 pA, p<0.01; green vs. purple means in *Figure 2E*). These numbers indicate a significant (about 1.5-fold) under-estimate of q values with the EPSC amplitude variance-mean analysis compared to direct measurements. Altogether these results indicate that the peak EPSC amplitude mean-variance analysis leads to over-estimates of P_1 and P_{max}, and to under-estimates of N and q, likely due to a combination of receptor saturation and synaptic jitter. Consequently, the difference between the moderate maximum P values found in this work, and higher values found in earlier studies, may partially arise from uncorrected errors linked to receptor saturation and synaptic jitter in these earlier studies.

Combining measurements of Ca²⁺ entry with P measurements

The above results show that values of P per release site are markedly smaller than 1. If the value of δ were 1, as is commonly assumed, then the low range of P values would predict that P is highly sensitive to Ca²⁺ entry, because the dose-response curve of release probability as a function of $[Ca^{2+}]_i$ is cooperative at the foot of the curve (*Dodge and Rahamimoff, 1967*; *Schneggenburger and Neher, 2000*). Therefore we next investigated the changes in Ca²⁺ entry associated with $[Ca^{2+}]_o$ changes and with TEA applications. For this purpose, we performed two-photon imaging of single PF varicosities (*Figure 3A*) to determine Ca²⁺ entry elicited by AP trains. We started fluorescence measurements about 30 min after establishing somatic whole-cell recording to allow dye equilibration in the imaged axonal area. Ca²⁺ entry was evaluated as the relative increase of the peak fluorescence measurement of OGB-6F ($\Delta F/F_0$: *Figure 3B*). *Figure 3B* shows an experiment where we compared $\Delta F/F_0$ signals under control conditions and during TEA application, finding a reversible increase. In conformity with previous results (*Sabatini and Regehr, 1997*; *Brenowitz and Regehr, 2007*; *Miki et al., 2016*), we found that the amount of Ca²⁺ entry per AP did not change significantly during an AP train (*Figure 3C*). Three series of experiments were performed: adding 1 mM TEA starting from a 1.5 mM $[Ca^{2+}]_o$ solution, as in panel B (n = 5); increasing the TEA concentration from 1 mM to 5
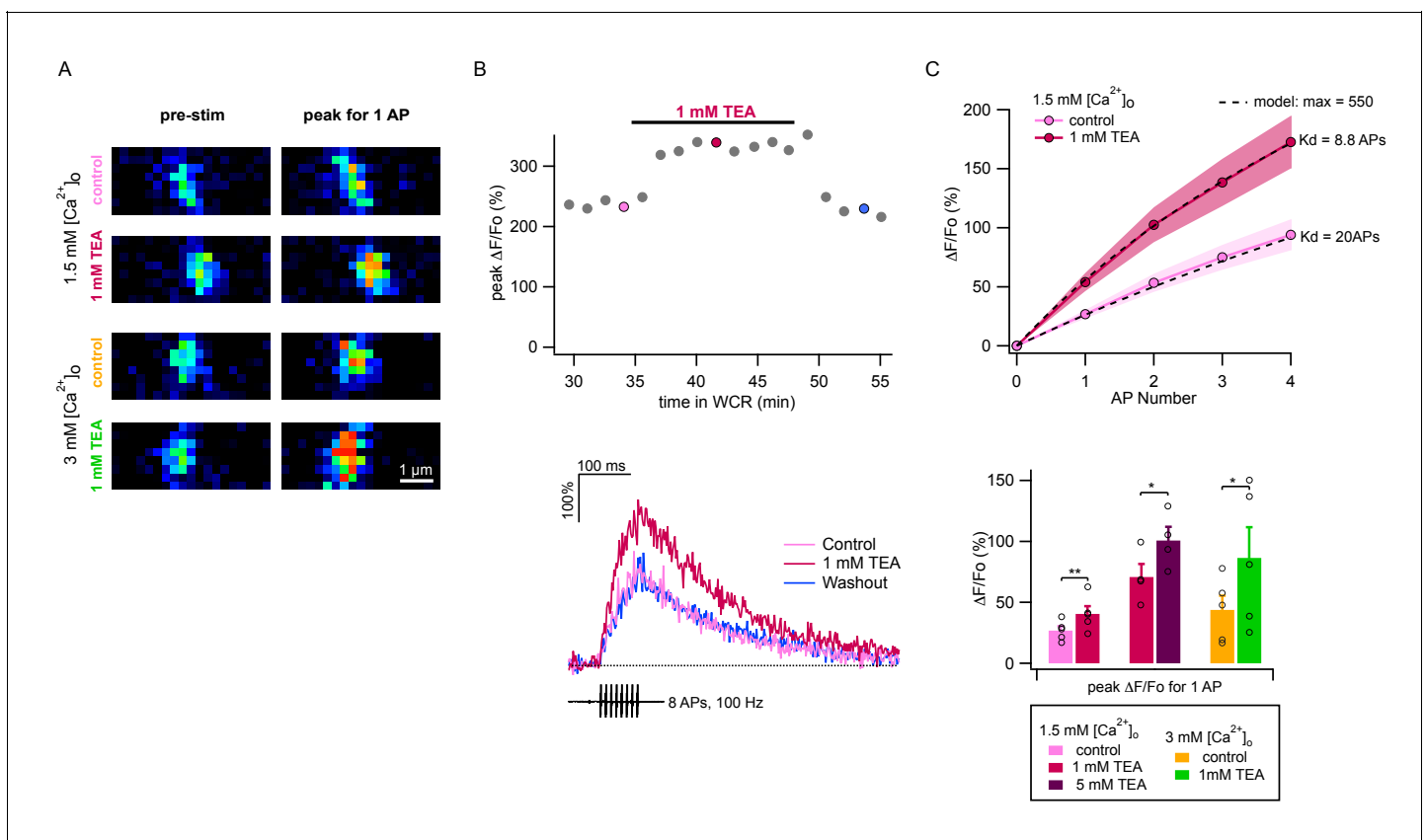
**Figure 3.** TEA augments AP-evoked Ca²⁺ rise in single PF varicosities. (**A**) Single scans of two representative varicosities (one in 1.5 mM $[Ca^{2+}]_o$ and the other in 3 mM $[Ca^{2+}]_o$), showing $[Ca^{2+}]_i$ signal at rest (left) and following a single AP (right), both in control conditions (upper panels) and the presence of 1 mM TEA (lower panels). Cells were loaded with 500 μM of the calcium indicator OGB-6F. In both cases TEA appears to increase the AP-driven $[Ca^{2+}]_i$ rise. (**B**) Top: Time-course of peak $\Delta F/F_0$ after 8 APs as a function of time in whole-cell recording. After a 30 min loading period the basal fluorescence was stable. 1 mM TEA was added at 35 min, causing an increase in the signal; the effect was reversible upon drug washout. Bottom: Time course of $\Delta F/F_0$ signal for individual responses during and after 8 AP stimulation; corresponding dots with same color coding in the upper plot. (**C**) Top: Average AP-evoked peak $\Delta F/F_0$ values as a function of AP number (shadowed colors indicate ± SEM; n = 5 varicosities in control, and n = 10 in 1 mM TEA). Dotted lines show fits of the data assuming constant Ca²⁺ entry per AP, using a hyperbolic function describing the sensitivity of OGB-6F on Ca²⁺ concentration (see Materials and methods; half saturation points are indicated next to each trace). Bottom: Average peak $\Delta F/F_0$ evoked by the first AP for each treatment. Circles show results from individual experiments. Bars show means ± SEM. Significant differences between mean values are illustrated (*: p<0.05; **: p<0.01; paired t-tests).

mM, starting in a 1.5 mM $[Ca^{2+}]_o$ plus 1 mM TEA solution (n = 4); and adding 1 mM TEA in 3 mM $[Ca^{2+}]_o$ (n = 5). Group results showed significant increases of Ca^{2+} entry upon application of 1 mM TEA, both when starting from a 1.5 mM $[Ca^{2+}]_o$ solution (control: 26.7 ± 3.6%; 1 mM TEA: 40.5 ± 3.6%; p<0.01, paired t-test) and when starting from a 3 mM $[Ca^{2+}]_o$ solution (control: 43.8 ± 11.6%; 1 mM TEA: 86.4 ± 25.2%; p<0.05; paired t-test; *Figure 3C*, lower panel). Likewise, we found a significant increase of fluorescence measurements in 1.5 mM $[Ca^{2+}]_o$ when increasing the TEA concentration from 1 to 5 mM (1 mM TEA: 70.8 ± 10.6%; 5 mM TEA: 100.7 ± 11.3%; p<0.05; paired t-test; *Figure 3C*, lower panel). Therefore, even though our previous results indicate that P_1 does not increase when elevating the TEA concentration from 1 to 5 mM, the present imaging results show that Ca^{2+} entry is substantially larger at the higher TEA concentration. The opposite situation is found when comparing results in the presence of 1 mM TEA and 3 mM $[Ca^{2+}]_o$ (green bar) with those in the presence of 5 mM TEA and 1.5 mM $[Ca^{2+}]_o$ (purple bar). Whereas P_1 is larger in the first solution than in the second (*Figure 1E*), $\Delta F/F_0$ signals appear similar (*Figure 3C*). Therefore altogether, comparison of the results in *Figure 1E* and *Figure 3C* reveals discrepancies between P_1 results and $\Delta F/F_0$ results, indicating that p, the release probability of docked SVs, is not the only determinant of P_1.

Modelling the $P_1([Ca^{2+}]_i)$ relation

Current models of SV release assume that a presynaptic AP induces a local $[Ca^{2+}]_i$ transient at the level of vesicular Ca^{2+} sensors with a sub-ms duration and an amplitude of several 10 s of µM (*Bollmann et al., 2000*; *Schneggenburger and Neher, 2000*). The Ca^{2+} sensors respond to the $[Ca^{2+}]_i$ transient with a sequence of fast Ca^{2+} binding to a series of 4–5 cooperative binding sites, followed by an irreversible exocytosis step (*Dodge and Rahamimoff, 1967*; *Wu and Saggau, 1994*; *Bollmann et al., 2000*; *Schneggenburger and Neher, 2000*; *Lou et al., 2005*). We found that depending on the mode of stimulation, such models predict different dose-response curves representing the synapse output as a function of peak global $[Ca^{2+}]_i$. In *Figure 4A–B*, we compare the dose-response curve for step $[Ca^{2+}]_i$ increases (*Figure 4A*) or for AP stimulations (*Figure 4B*), using $[Ca^{2+}]_{li}$-sensitive reaction steps and $[Ca^{2+}]_i$ profiles previously developed to simulate release at PF-MLI synapses (*Miki et al., 2018*). Even though Ca^{2+}-sensitive reaction steps are the same for the two sets of simulations both using a modified version of the allosteric model of *Lou et al. (2005)*, as explained in *Miki et al. (2018)*, the dose-response curve is markedly steeper in response to step $[Ca^{2+}]_i$ increases (with an apparent Hill coefficient n = 3; *Figure 4A*) than in response to AP stimulations (with an apparent Hill coefficient n = 1.7; *Figure 4B*). The difference reflects the fact that in AP-induced responses, effective calcium levels vary in a complex manner with calcium entry, due to the diffusion of entering calcium ions and of their interaction with a variety of calcium buffers. These simulations indicate that the Hill coefficient of the dose-response curve does not depend only on the number of Ca^{2+} binding steps in the kinetic model (5 in the present case), but also on the mode of stimulation (Ca^{2+} uncaging vs. AP).

Next, we asked how the dose-response curve of *Figure 4B* could be used to estimate δ. For this purpose, we combined together P_1 values obtained under the various experimental conditions of *Figure 1*, together with peak global $[Ca^{2+}]_l$ data obtained from *Figure 3*, creating an experimental plot of P_1 as a function of peak global $[Ca^{2+}]_l$ (*Figure 4C*). In this plot, P_1 values are overall means derived from the paired control/TEA experiments of *Figure 1* as well as from other experiments including the TEA/(TEA + 4-AP) experiments to be described below. In addition, P_1 values were corrected to only incorporate release events coming directly from docking sites ('one-step release'), as opposed to indirect release events coming from replacement sites ('two-step release': *Miki et al., 2018*). Because 2-step release events do not originate from docked SVs, they should not be considered in the estimate of δ. Fortunately, in ordinary experimental conditions, 2-step release appears only starting from the 2nd AP in a train, and is not detectable after the 1st AP. In these cases, no correction for P_1 is needed to account for 2-step release. Only in the most extreme condition of 3 mM $[Ca^{2+}]_o$ + TEA was a correction necessary (by 18%). Also, peak global values from *Figure 3C* were corrected for partial dye saturation. To relate the corrected experimental results in *Figure 4C* to the simulation in *Figure 4B*, we note that in *Figure 4B*, the ordinate is p, the release probability of docked SVs, whereas in *Figure 4C*, the ordinate is P_1, the global release probability in response to the first stimulus in a train. As already pointed out, P_1 data points incorporate both δ and p factors, according to the relation $P_1 = \delta$ p. Clearly, P_1 data differ from the curve in *Figure 4B* and
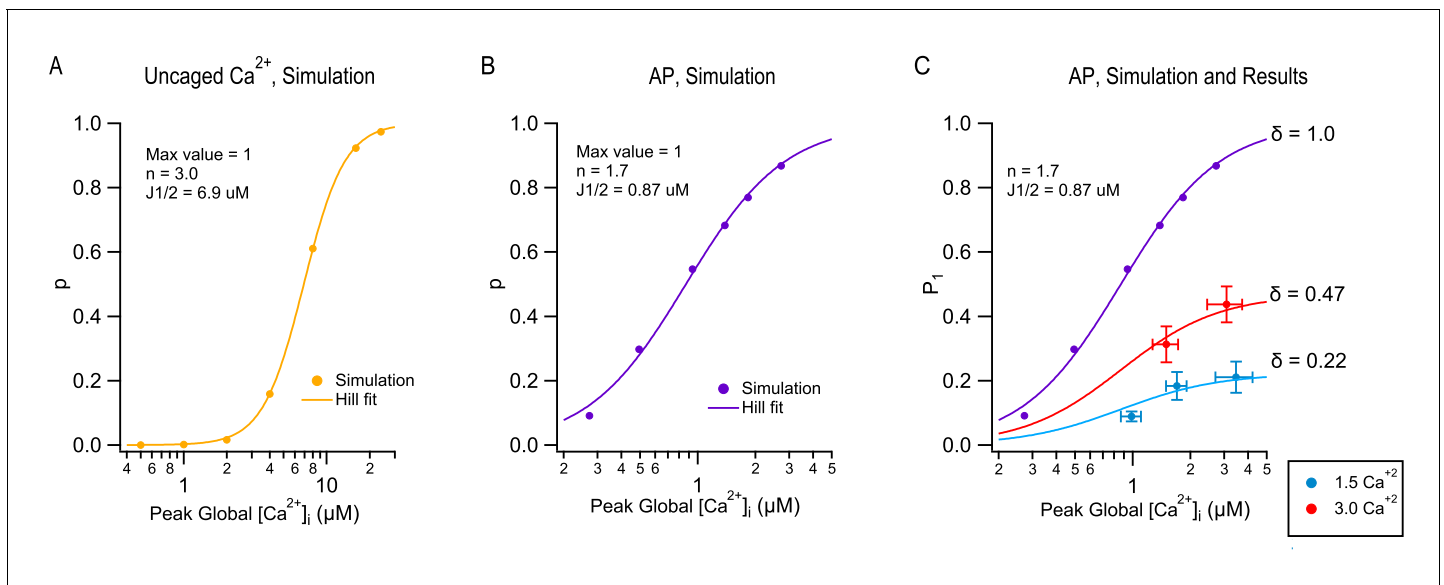
Figure 4. Modeling TEA-induced P increases in 1.5 mM $[Ca^{2+}]_o$ and in 3 mM $[Ca^{2+}]_o$. (A) Plot of the release probability (p) as a function of step $[Ca^{2+}]_i$ increases, as predicted by the allosteric vesicular release model of *Lou et al. (2005)*, modified as explained in *Miki et al. (2018)*. (B) The same model predicts a different dose-response curve when plotting the release probability of a docked SV as a function of peak global $[Ca^{2+}]_i$ following an AP stimulation, by varying the total amount of Ca^{2+} entry per AP. For this simulation the Ca^{2+} diffusion and buffering model developed earlier for PF-MLI synapses was used (*Miki et al., 2018*). Note the more shallow dose-response curve (Hill coefficient: 1.7 vs. 3.0) and higher apparent affinity ($J_{1/2}$: 0.87 µM vs. 6.9 µM) with AP stimulation compared to step $[Ca^{2+}]_i$ stimulation. (C) Combining together the results of *Figure 1* and of *Figure 3* for the first stimulation in a train produces a plot of P_1 as a function of peak global $[Ca^{2+}]_i$, both at 1.5 mM $[Ca^{2+}]_o$ (blue: no TEA, 1 mM TEA, and 5 mM TEA) and at 3 mM $[Ca^{2+}]_o$ (red: no TEA, and 1 mM TEA). These data cannot be fit directly with the dose-response curve in (B) (purple), but they can be fit using two different scaled versions of this curve, giving $\delta = 0.22$ in 1.5 mM $[Ca^{2+}]_o$ and $\delta = 0.47$ in 3 mM $[Ca^{2+}]_o$.

The online version of this article includes the following figure supplement(s) for figure 4:

Figure supplement 1. Effect of 4-AP on release.

furthermore, they cannot be fit from this curve by using a single scaling factor. However, acceptable fits are obtained when using two different scalings depending on $[Ca^{2+}]_o$ (*Figure 4C*). In these plots, δ appears as the asymptotic value of P_1 at high global $[Ca^{2+}]_i$, yielding $\delta = 0.22$ at 1.5 mM $[Ca^{2+}]_o$ and $\delta = 0.47$ at 3 mM $[Ca^{2+}]_o$ (*Figure 4C*). Altogether this analysis suggests that δ values increase as a function of $[Ca^{2+}]_o$ and therefore, that changes in both δ and p contribute to the sensitivity of P as a function of $[Ca^{2+}]_o$.

Combined effects of TEA and 4-AP

It may be asked whether the above results may be extended to other blockers of potassium channels than TEA. Both in MLI terminals and in the calyx of Held, 4-AP increases synaptic transmission more efficiently than TEA (*Tan and Llano, 1999*; *Ishikawa et al., 2003*). In MLI terminals, 4-aminopyridine (4-AP) markedly increases calcium entry whereas TEA alone is almost ineffective; combining TEA and 4-AP together leads to an even larger AP-induced calcium elevation than when applying 4-AP alone (*Tan and Llano, 1999*). In view of these earlier results, we expected that combining TEA and 4-AP in our preparation should lead to a very large presynaptic calcium entry. Nevertheless, supposing that the model of *Figure 4* is valid, P_1 should not be able to increase beyond the value of δ. Group results showed P_1 values of 0.140 ± 0.053 in 1.5 mM $[Ca^{2+}]_o$ and 1 mM TEA without 4-AP, and of 0.187 ± 0.048 after further addition of 15 µM 4-AP (*Figure 4—figure supplement 1*). After adding 4-AP, both 2-step release and facilitation were very pronounced, probably due to a marked increase in calcium entry. After correction for 2-step release, P_1 in TEA + 4-AP was 0.125 ± 0.032, a value similar to that in TEA alone. Meanwhile, P_{max} increased from 0.263 ± 0.046 in TEA alone to 0.550 ± 0.149 in TEA + 4-AP (*Figure 4—figure supplement 1*), a value similar to that obtained in 3 mM $[Ca^{2+}]_o$ and 1 mM TEA (*Figure 1*). Thus, while P_1 was limited by the resting docking site occupancy, the synapse could deliver more SVs upon repetitive stimulation as SV replenishment was

increased. In conclusion, whether calcium entry is increased with TEA alone or with a combination of TEA and 4-AP, P_1 remains limited by the value of δ.

Discussion

Main finding

In the present work we take advantage of the recently developed method of SV counting (*Malagon et al., 2016*) to examine variations of the release probability of single docking sites (P) during short term synaptic plasticity, following addition of TEA, and when changing $[Ca^{2+}]_o$. Our main finding is that the synaptic strength at the beginning of an AP train (P_1) has a maximum attainable value that depends on the value of $[Ca^{2+}]_o$. With 1.5 mM $[Ca^{2+}]_o$, the maximum of P_1 is 0.22 SV per AP and per release/docking site, whereas with 3 mM $[Ca^{2+}]_o$, the maximum of P_1 is 0.47.

Our interpretation of this finding is that when the release probability of docked SVs, p, is close to 1, P_1 is limited by the resting docking site probability δ, and that δ is lower in 1.5 mM $[Ca^{2+}]_o$ compared to 3 mM $[Ca^{2+}]_o$. The maximum output per site gives an estimate of resting docking site occupancy, a basic parameter of synaptic function that has been difficult to evaluate.

Correcting release probability for docking site occupancy

Our results confirm earlier suggestions that δ is less than 1 at PF-MLI synapses (*Miki et al., 2016*; *Miki et al., 2018*). In addition, we now provide reliable δ estimates. The present finding that $\delta = 0.22$ under physiological conditions (1.5 mM $[Ca^{2+}]_o$) implies that there is a large discrepancy between the release probability per docking site, P_1, and the release probability per occupied docking site, p. By inverting the $P_1 = \delta p$ relation, we obtain from $P_1 = 0.089$ and $\delta = 0.22$ that $p = 0.39$ in 1.5 mM $[Ca^{2+}]_o$. At 3 mM $[Ca^{2+}]_o$, we have $P_1 = 0.28$ and $\delta = 0.47$, so that $p = 0.60$. Therefore both at 1.5 mM $[Ca^{2+}]_o$ and at 3 mM $[Ca^{2+}]_o$, the actual release probability of docked SVs is substantially higher than it would appear without the correction. In the presence of TEA, p values calculated from the pooled data of *Figure 4* approach 1 (1.5 mM $[Ca^{2+}]_o$: $p = 0.85$ in 1 mM TEA and $p = 0.95$ in 5 mM TEA; 3 mM $[Ca^{2+}]_o$: $p = 0.89$ in 1 mM TEA, value corrected for 2-step release). Therefore in the present preparation, P_1 values in the presence of TEA give reasonably good approximations of δ.

This correction is important when relating release probability and local calcium profiles. For example, at synapses between PFs and Purkinje cells, P values are comparatively small, yet EGTA application experiments suggest tight coupling between SVs and Ca^{2+} entry, indicating high p values (*Schmidt et al., 2013*). A low δ value at these synapses, similar to the value found here for PF-MLI synapses, is a plausible explanation for these apparently discrepant results.

Comparison with other preparations

Increasing evidence suggests that part of inter-synaptic variability may reside in differences in docking site occupancy. Specifically, synapses follow a gradient from low release probability, facilitating synapses to high release probability, depressing synapses, presumably depending on the proportion of occupancy of release sites by SVs (*Pan and Zucker, 2009*; *Pulido and Marty, 2018*; *Neher and Brose, 2018*). PF-MLI synapses have a low δ value in normal physiological conditions (0.22 at 1.5 mM $[Ca^{2+}]_o$ according to the present study) and are facilitating, indicating that they belong to the first category, called 'tonic synapses' (*Pan and Zucker, 2009*; *Neher and Brose, 2018*). By contrast, SV release statistics at simple MLI-MLI synapses indicate a higher resting δ value near 0.5–0.7 in 2 mM $[Ca^{2+}]_o$ (*Trigo et al., 2012*; *Pulido et al., 2015*). Furthermore MLI-MLI synapses are depressing, and altogether MLI-MLI synapses appear closer to the 'phasic synapse' category (*Pan and Zucker, 2009*; *Neher and Brose, 2018*).

Because of the difficulty of separating δ from p, estimates of δ in most preparations are not available. Nevertheless, earlier variance/mean analysis studies, often carried out on peak synaptic current amplitudes, give constraints on δ. Maximum P values reported in these studies are usually in the range 0.5–1 (*Branco and Staras, 2009*). In view of the relation $P = \delta p$, since $p<1$, such large P values suggest resting δ values above 0.5. However these maximum P values are almost always obtained in high $[Ca^{2+}]_o$ conditions (calyx of Held: *Taschenberger et al., 2005*; PF-MLI synapses: *Ishiyama et al., 2014*; fly neuromuscular junction: *Reddy-Alla et al., 2017*; hippocampal cultures:

Sakamoto et al., 2018). In view of the present evidence that δ increases as a function of $[Ca^{2+}]_o$, the high P values at high $[Ca^{2+}]_o$ are compatible with δ values < 0.5 under normal $[Ca^{2+}]_o$ conditions, at least in some (tonic) synapses. Apart from using high $[Ca^{2+}]_o$ conditions, another factor that may have contributed in some studies to high apparent P values is uncorrected synaptic jitter and receptor saturation, as documented above (*Figure 2*). One notable exception is the climbing fibre-Purkinje cell synapse, that may represent an extreme case of phasic synapses, and that exhibits P values above 0.9 at normal $[Ca^{2+}]_o$ (*Silver et al., 1998*). Overall our conclusions appear well compatible with earlier P estimates obtained with variance/mean analysis of peak synaptic current amplitudes.

Possible mechanisms of changes of δ with $[Ca^{2+}]_o$

An increase in $[Ca^{2+}]_o$ likely acts on the docking site occupancy by inducing an increase in $[Ca^{2+}]_i$ after reequilibration of the cytosolic Ca^{2+} concentration. It is widely accepted that following docking site depletion, docking site replenishment is sensitive to the bulk $[Ca^{2+}]_i$ (*Neher and Sakaba, 2008*). This suggests that the proportion of occupied docking sites at rest may be enhanced by a $[Ca^{2+}]_i$ increase, as the equilibrium is shifted in favor of SV binding to the docking site. Recent electron microscopy studies are in accord with this proposal (*Chang et al., 2018*; *Kusick et al., 2018*). Several AZ molecules could be responsible for Ca^{2+}-dependent SV docking, including synaptotagmin-1 (*Chang et al., 2018*) and Munc13 (*Shin et al., 2010*). Another possibility is that Ca^{2+}-dependent SV docking is due to activation of actomyosin-driven SV movement by $[Ca^{2+}]_i$ (*Lee et al., 2012*; *Miki et al., 2016*).

Physiological relevance

A $[Ca^{2+}]_i$ –induced change in resting docking site occupancy may not only apply when changing $[Ca^{2+}]_o$, as proposed in the present work, but it may also occur following a number of other manipulations leading to a change in the global presynaptic $[Ca^{2+}]_i$ concentration. In the calyx of Held, as well as in MLI terminals, subthreshold presynaptic depolarization activates low-threshold voltage-gated Ca^{2+} channels, thus increasing release probability (*Awatramani et al., 2005*; *Bouhours et al., 2011*). Activation of Cl⁻-permeant presynaptic glycinergic or GABAergic receptors in these synapses engages this pathway, leading to a presynaptic $[Ca^{2+}]_i$ increase and to an enhancement of synaptic strength (*Turecek and Trussell, 2001*; *Trigo et al., 2007*; *Zorrilla de San Martin et al., 2017*). Activation of cationic channels by presynaptic nicotinic receptors, AMPA receptors, or NMDA receptors, is also able to increase presynaptic $[Ca^{2+}]_i$, in various preparations including MLI terminals, and these actions have been shown to increase release (*Sharma and Vijayaraghavan, 2003*; *Rossi et al., 2008*; *Rossi et al., 2012*). Finally, enhancement of neurotransmitter release by passive spread of subthreshold somatic depolarization in hippocampal and cortical synapses ('analog signaling') depends on an increase in presynaptic $[Ca^{2+}]_i$ concentration (*Shu et al., 2006*; *Alle and Geiger, 2006*). In view of the present results, it is possible that these effects are mediated at least in part by an increase in resting docking site occupancy. Altogether, $[Ca^{2+}]_i$-driven changes of docking site occupancy appears as a simple and powerful mechanism of gain control of synaptic strength that may be used by various forms of neuromodulation.

Materials and methods

Recording procedures

Sagittal slices (200 µm thick) were prepared from the cerebellar vermis of Sprague-Dawley rats (P12–P17) following the animal care guidelines of Paris Descartes University (approval no. A-750607). Recordings were obtained from either basket or stellate cells in the molecular layer; these cells were collectively called molecular layer interneurons (MLIs). The composition of the extracellular solution was (in mM): 130 NaCl, 2.5 KCl, 26 NaHCO$_3$, 1.3 NaH$_2$PO$_4$, 10 glucose, 2 CaCl$_2$, and 1 MgCl$_2$ (osmolarity: 300 mosm). This solution was equilibrated with 95% O$_2$ and 5% CO$_2$ (pH 7.4). The internal recording solution contained (in mM): 144 K-gluconate, 6 KCl, 4.6 MgCl$_2$, 1 EGTA, 0.1 CaCl$_2$, 10 HEPES, 4 ATP-Na, 0.4 GTA-Na; pH 7.3 (osmolarity: 300 mosm). Recordings were at 30–34˚C.

Simple synapse recording

To study simple PF-MLI synapses, potential postsynaptic MLIs were recorded under voltage clamp at –60 mV. For extracellular stimulation, a monopolar pipette was filled with internal solution. NMDA receptors and GABA$_A$ receptors were blocked by inclusion of D(–)−2-amino-5-phosphonopentanoic acid (APV, 50 µM) and gabazine (15 µM). Two alternative procedures were used to find an appropriate location for electrical stimulation. In the first procedure, an electrical stimulation pipette was located in the molecular layer, above the dendritic field of the recorded MLI, and the pipette position and stimulation strength were adjusted to obtain minimal stimulation (*Miki et al., 2016*). In the second procedure, we puff-applied the internal solution including 150 mM K$^+$ from a pipette using small pressure steps while moving the pipette in the granule cell layer (*Miki et al., 2017*). When we found a burst-like EPSC response in the postsynaptic cell, we reduced the pressure of puffing to better define the spot for stimulation. Then we switched to electrical stimulation, using the same pipette, and we adjusted stimulation intensity to fire a connected granule cell under minimal stimulation conditions. With either procedure, definitive acceptance of the experiment as a usable simple synapse recording occurred after analysis and depended on three criteria (*Malagon et al., 2016*): (i) a decrement of EPSC amplitudes of second events in a pair, reflecting activation of a common set of receptors belonging to one PSD; (ii) a Gaussian distribution of EPSC amplitudes with a coefficient of variation (CV) less than 0.5; and (iii) stability of the overall responsiveness over time. Single stimulations and trains of two or eight stimulation pulses were applied repetitively with intervals of 10 s between sweeps. Statistical data were derived from sequences of 10–30 trains.

Decomposition of EPSCs

We determined occurrence times of individual EPSCs based on deconvolution analysis, as detailed in *Malagon et al. (2016)*, and we built latency distributions by averaging the occurrence times across experiments. We briefly describe the analysis here. Firstly, we made an average of single EPSCs obtained during asynchronous release to obtain a template in a given synapse. Then the average mEPSC was fit by triple-exponential function with five free parameters (rise time, amplitude, fast decay time constant, slow decay time constant, and amplitude fraction of slow decay). Next, mEPSC and individual data traces were deconvolved using the five parameters. The deconvolved mEPSC resulted in a narrow spike, and the deconvolved data traces resulted in sequences of spikes. Finally, we fit a given deconvolved trace by a sum of scaled narrow spikes in order to obtain the timing of each event. The amplitude parameter was free because the peak EPSC amplitude varied during a train due to receptor saturation and desensitization. The above procedure had a detection limit that caused a failure of separation of two events occurring within 0.2 ms. To correct for missed events, we split into two the events having amplitudes at least 1.7 times larger than the average amplitude obtained during asynchronous release.

Pharmacological manipulations

In TEA experiments, we checked somatic potassium currents by applying 3 ms voltage step to 0 mV until TEA reduced potassium current amplitudes to a stable level, and then we started to collect data.

Ca^{2+} imaging of presynaptic varicosities

For Ca^{2+} imaging experiments, sagittal (200 µm) slices were prepared using a modified extracellular saline, as detailed in *Brenowitz and Regehr (2007)*. Experiments were conducted in the same conditions as in the electrophysiology experiments (32–34°C, with the 3 mM extracellular Ca^{2+} saline including APV and gabazine). Granule cells were loaded under whole-cell recording with a solution containing (in mM): 140 K-gluconate, 5.4 KCl, 4.1 MgCl$_2$, 9.9 HEPES, 0.36 Na-GTP, 3.6 Na-ATP, 500 µM of Oregon green 488 BAPTA-6F (OGB-6F: K$_d$ for calcium of 5.1 µM; Invitrogen) and 20 µM Alexa-594 (Invitrogen). Imaging was performed with a custom-built 2-photon system, with 820 nm excitation provided by a MaiTai-Sapphire laser (Spectra Physics, USA). In order to visualize the granule cell axon, large raster scans were performed while acquiring the Alexa 594 fluorescence with a red channel photomultiplier (Hamamatsu H7422 PA-sel, bandpass emission filter 635 ± 65 nm, Chroma Technology; or avalanche photodiode Perkin Elmer, SPCM-AQR-13). Single varicosity imaging was performed using raster scans of 5 by 2 µm dimensions at dwell times of 2 ms. The granule

cells were kept under current clamp conditions. We found that keeping a hyperpolarized holding potential improved recording stability, so that resting membrane potential was kept around –90 mV. APs were evoked by 1 ms steps of 350–500 pA. Stimulation protocols were 4 or 8 APs at 100 Hz and were repeated every 1 min. Calcium signaling was analyzed in the pixels encompassing the varicosity in terms of fluorescence changes relative to pre-stimulus values ($\Delta F/F_o$, expressed in %) with software written in the Igor Pro programming environment (Wavemetric, Lake Oswego, OR, USA).

To fit the data in *Figure 3C*, we assumed gradual saturation of OGB-6F as a function of Ca^{2+} entry, with equal contributions for each AP (*Miki et al., 2016*). Estimated K_d values are indicated in *Figure 3C*, upper panel. As before, dye saturation was set at 6.5 times the baseline level (*Miki et al., 2016*). The data in *Figure 4C* are based on the pooled data in the lower panel of *Figure 3C*, after correcting for dye saturation.

Simulations

We calculated the release probabilities for various Ca^{2+} waveforms by numerical integration of differential equations using Igor Pro with a time interval of 0.001 ms as described (*Miki et al., 2018*). We performed the simulations using a simple one-step release model without replenishment at docking sites (*Miki et al., 2018*, *Figure 1*) with the allosteric model of *Lou et al. (2005)*. According to the fit of data in *Miki et al. (2018)*, we used the following parameter values for the allosteric model: K_{on} = 5×10⁸ $M^{-1}s^{-1}$, K_{off} = 5000 s^{-1}, b = 0.75, γ = 1500 s^{-1}, and f = 31.1. γ is the fusion rate of the 5Ca-binding state (V_{5Ca}), which is identical to $l_+ \times f^5$. f is a factor determining the increase in vesicle fusion rate upon Ca^{2+} binding. The fusion rate at $V_{0Ca-4Ca}$ is $l_+ \times f^{0-4}$. b is a cooperativity factor (*Lou et al., 2005*). In *Figure 4A-B*, the probability of occupancy at docking site was set to 1. For the Ca^{2+} uncaging simulation, we assumed step $[Ca^{2+}]$ increases from a basal $[Ca^{2+}]$ of 50 nM to 0.5, 1, 2, 4, 8, 16, or 24 µM, and we calculated the release probabilities by dividing the total number of vesicle release between 0 and 5 ms by the docking site number. For the AP simulation, we used the local $[Ca^{2+}]$ obtained from Ca^{2+} simulation at 40 nm distance from the nearest Ca^{2+} channels (*Miki et al., 2018*). Global $[Ca^{2+}]$ was obtained at the center of a bouton in Ca^{2+} simulation. The Ca^{2+} simulation was described in detail in a previous report (*Miki et al., 2018*). Briefly, we calculated the spatiotemporal distribution of $[Ca^{2+}]$ at a PF bouton. We used the bouton size of 0.9 × 0.5×0.5 µm³ cuboid, and the Ca^{2+} channel distributions based on the electron microscopy observations (*Miki et al., 2017*; *Miki et al., 2018*). The amplitude of Ca^{2+} influx through each channel during an AP was set at 0.2 pA and a fraction of channel open probability during an AP of ~0.7. We assumed a Gaussian-shaped Ca^{2+} influx with a half-amplitude duration of 0.34 ms. Other model parameters were set following *Miki et al. (2018)*. To create Ca^{2+} waveforms having various amplitudes for the AP simulation, we multiplied the simulated local and global $[Ca^{2+}]$ by a factor of 0.25, 0.5, 1, 1.5, 2 and 3 while keeping the resting $[Ca^{2+}]$ of 50 nM. We calculated the release probabilities by dividing the total number of vesicle release between 0 and 5 ms after the beginning of the local $[Ca^{2+}]$ increase by the number of docking sites.

Additional information

Decision letter and Author response
Decision letter https://doi.org/10.7554/eLife.52137.sa1
Author response https://doi.org/10.7554/eLife.52137.sa2

Additional files

Supplementary files
- Source data 1. Igor figure files.
- Transparent reporting form

Data availability
An additional file called 'Source data 1' contains original data as well as analysis for this article.

References

Alle H, Geiger JR. 2006. Combined analog and action potential coding in hippocampal mossy fibers. *Science* **311**:1290–1293. DOI: https://doi.org/10.1126/science.1119055, PMID: 16513983

Awatramani GB, Price GD, Trussell LO. 2005. Modulation of transmitter release by presynaptic resting potential and background calcium levels. *Neuron* **48**:109–121. DOI: https://doi.org/10.1016/j.neuron.2005.08.038, PMID: 16202712

Bollmann JH, Sakmann B, Borst JG. 2000. Calcium sensitivity of glutamate release in a calyx-type terminal. *Science* **289**:953–957. DOI: https://doi.org/10.1126/science.289.5481.953, PMID: 10937999

Bouhours B, Trigo FF, Marty A. 2011. Somatic depolarization enhances GABA release in cerebellar interneurons via a calcium/protein kinase C pathway. *Journal of Neuroscience* **31**:5804–5815. DOI: https://doi.org/10.1523/JNEUROSCI.5127-10.2011, PMID: 21490222

Branco T, Staras K. 2009. The probability of neurotransmitter release: variability and feedback control at single synapses. *Nature Reviews Neuroscience* **10**:373–383. DOI: https://doi.org/10.1038/nrn2634, PMID: 19377502

Brenowitz SD, Regehr WG. 2007. Reliability and heterogeneity of calcium signaling at single presynaptic boutons of cerebellar granule cells. *Journal of Neuroscience* **27**:7888–7898. DOI: https://doi.org/10.1523/JNEUROSCI.1064-07.2007, PMID: 17652580

Chang S, Trimbuch T, Rosenmund C. 2018. Synaptotagmin-1 drives synchronous Ca2+-triggered fusion by C2B-domain-mediated synaptic-vesicle-membrane attachment. *Nature Neuroscience* **21**:33–40. DOI: https://doi.org/10.1038/s41593-017-0037-5, PMID: 29230057

Clements JD. 2003. Variance-mean analysis: a simple and reliable approach for investigating synaptic transmission and modulation. *Journal of Neuroscience Methods* **130**:115–125. DOI: https://doi.org/10.1016/j.jneumeth.2003.09.019, PMID: 14667541

Dodge FA, Rahamimoff R. 1967. Co-operative action a calcium ions in transmitter release at the neuromuscular junction. *The Journal of Physiology* **193**:419–432. DOI: https://doi.org/10.1113/jphysiol.1967.sp008367, PMID: 6065887

Hallermann S, Fejtova A, Schmidt H, Weyhersmüller A, Silver RA, Gundelfinger ED, Eilers J. 2010. Bassoon speeds vesicle reloading at a central excitatory synapse. *Neuron* **68**:710–723. DOI: https://doi.org/10.1016/j.neuron.2010.10.026, PMID: 21092860

Ishikawa T, Nakamura Y, Saitoh N, Li WB, Iwasaki S, Takahashi T. 2003. Distinct roles of Kv1 and Kv3 potassium channels at the Calyx of held presynaptic terminal. *The Journal of Neuroscience* **23**:10445–10453. DOI: https://doi.org/10.1523/JNEUROSCI.23-32-10445.2003, PMID: 14614103

Ishiyama S, Schmidt H, Cooper BH, Brose N, Eilers J. 2014. Munc13-3 superprimes synaptic vesicles at granule cell-to-basket cell synapses in the mouse cerebellum. *Journal of Neuroscience* **34**:14687–14696. DOI: https://doi.org/10.1523/JNEUROSCI.2060-14.2014, PMID: 25355221

Jahn R, Fasshauer D. 2012. Molecular machines governing exocytosis of synaptic vesicles. *Nature* **490**:201–207. DOI: https://doi.org/10.1038/nature11320, PMID: 23060190

Kawaguchi SY, Sakaba T. 2017. Fast Ca2+ Buffer-Dependent Reliable but Plastic Transmission at Small CNS Synapses Revealed by Direct Bouton Recording. *Cell Reports* **21**:3338–3345. DOI: https://doi.org/10.1016/j.celrep.2017.11.072, PMID: 29262314

Kusick GF, Chin M, Lippmann K, Adula KP, Davis WM, Jorgensen EM, Watanabe S. 2018. Synaptic vesicles undock and then transiently dock after an action potential. *bioRxiv*. DOI: https://doi.org/10.1101/509216

Lee JS, Ho WK, Lee SH. 2012. Actin-dependent rapid recruitment of reluctant synaptic vesicles into a fast-releasing vesicle pool. *PNAS* **109**:e765–e774. DOI: https://doi.org/10.1073/pnas.1114072109, PMID: 22393020

Llano I, González J, Caputo C, Lai FA, Blayney LM, Tan YP, Marty A. 2000. Presynaptic calcium stores underlie large-amplitude miniature IPSCs and spontaneous calcium transients. *Nature Neuroscience* **3**:1256–1265. DOI: https://doi.org/10.1038/81781, PMID: 11100146

Llano I, Gerschenfeld HM. 1993. Inhibitory synaptic currents in stellate cells of rat cerebellar slices. *The Journal of Physiology* **468**:177–200. DOI: https://doi.org/10.1113/jphysiol.1993.sp019766, PMID: 7504726

Lou X, Scheuss V, Schneggenburger R. 2005. Allosteric modulation of the presynaptic Ca2+ sensor for vesicle fusion. *Nature* **435**:497–501. DOI: https://doi.org/10.1038/nature03568, PMID: 15917809

Malagon G, Miki T, Llano I, Neher E, Marty A. 2016. Counting vesicular release events reveals binomial release statistics at single glutamatergic synapses. *The Journal of Neuroscience* **36**:4010–4025. DOI: https://doi.org/10.1523/JNEUROSCI.4352-15.2016, PMID: 27053208

Midorikawa M, Sakaba T. 2015. Imaging exocytosis of single synaptic vesicles at a fast CNS presynaptic terminal. *Neuron* **88**:492–498. DOI: https://doi.org/10.1016/j.neuron.2015.09.047, PMID: 26539890

Miki T, Malagon G, Pulido C, Llano I, Neher E, Marty A. 2016. Actin- and Myosin-Dependent vesicle loading of presynaptic docking sites prior to exocytosis. *Neuron* **91**:808–823. DOI: https://doi.org/10.1016/j.neuron.2016.07.033, PMID: 27537485

Miki T, Kaufmann WA, Malagon G, Gomez L, Tabuchi K, Watanabe M, Shigemoto R, Marty A. 2017. Numbers of presynaptic Ca^{2+} channel clusters match those of functionally defined vesicular docking sites in single central synapses. *PNAS* **114**:E5246–E5255. DOI: https://doi.org/10.1073/pnas.1704470114, PMID: 28607047

Miki T, Nakamura Y, Malagon G, Neher E, Marty A. 2018. Two-component latency distributions indicate two-step vesicular release at simple glutamatergic synapses. *Nature Communications* **9**:3943. DOI: https://doi.org/10.1038/s41467-018-06336-5, PMID: 30258069

Miki T. 2019. What we can learn from cumulative numbers of vesicular release events. *Frontiers in Cellular Neuroscience* **13**:257. DOI: https://doi.org/10.3389/fncel.2019.00257, PMID: 31293386

Neher E, Brose N. 2018. Dynamically primed synaptic vesicle states: key to understand synaptic short-term plasticity. *Neuron* **19**:1283–1291. DOI: https://doi.org/10.1016/j.neuron.2018.11.024

Neher E, Sakaba T. 2008. Multiple roles of calcium ions in the regulation of neurotransmitter release. *Neuron* **59**:861–872. DOI: https://doi.org/10.1016/j.neuron.2008.08.019, PMID: 18817727

Pan B, Zucker RS. 2009. A general model of synaptic transmission and short-term plasticity. *Neuron* **62**:539–554. DOI: https://doi.org/10.1016/j.neuron.2009.03.025, PMID: 19477155

Pulido C, Trigo FF, Llano I, Marty A. 2015. Vesicular release statistics and unitary postsynaptic current at single GABAergic synapses. *Neuron* **85**:159–172. DOI: https://doi.org/10.1016/j.neuron.2014.12.006, PMID: 25543456

Pulido C, Marty A. 2017. Quantal Fluctuations in Central Mammalian Synapses: Functional Role of Vesicular Docking Sites. *Physiological Reviews* **97**:1403–1430. DOI: https://doi.org/10.1152/physrev.00032.2016

Pulido C, Marty A. 2018. A two-step docking site model predicting different short-term synaptic plasticity patterns. *The Journal of General Physiology* **150**:1107–1124. DOI: https://doi.org/10.1085/jgp.201812072, PMID: 29950400

Quastel DM. 1997. The binomial model in fluctuation analysis of quantal neurotransmitter release. *Biophysical Journal* **72**:728–753. DOI: https://doi.org/10.1016/S0006-3495(97)78709-5, PMID: 9017200

Reddy-Alla S, Böhme MA, Reynolds E, Beis C, Grasskamp AT, Mampell MM, Maglione M, Jusyte M, Rey U, Babikir H, McCarthy AW, Quentin C, Matkovic T, Bergeron DD, Mushtaq Z, Göttfert F, Owald D, Mielke T, Hell SW, Sigrist SJ, et al. 2017. Stable positioning of Unc13 restricts synaptic vesicle fusion to defined release sites to promote synchronous neurotransmission. *Neuron* **95**:1350–1364. DOI: https://doi.org/10.1016/j.neuron.2017.08.016, PMID: 28867551

Rossi B, Maton G, Collin T. 2008. Calcium-permeable presynaptic AMPA receptors in cerebellar molecular layer interneurones. *The Journal of Physiology* **586**:5129–5145. DOI: https://doi.org/10.1113/jphysiol.2008.159921, PMID: 18772200

Rossi B, Ogden D, Llano I, Tan YP, Marty A, Collin T. 2012. Current and calcium responses to local activation of axonal NMDA receptors in developing cerebellar molecular layer interneurons. *PLOS ONE* **7**:e39983. DOI: https://doi.org/10.1371/journal.pone.0039983, PMID: 22761940

Sabatini BL, Regehr WG. 1997. Control of neurotransmitter release by Presynaptic waveform at the granule cell to purkinje cell synapse. *The Journal of Neuroscience* **17**:3425–3435. DOI: https://doi.org/10.1523/JNEUROSCI.17-10-03425.1997, PMID: 9133368

Sakamoto H, Ariyoshi T, Kimpara N, Sugao K, Taiko I, Takikawa K, Asanuma D, Namiki S, Hirose K. 2018. Synaptic weight set by Munc13-1 supramolecular assemblies. *Nature Neuroscience* **21**:41–49. DOI: https://doi.org/10.1038/s41593-017-0041-9, PMID: 29230050

Saviane C, Silver RA. 2006. Fast vesicle reloading and a large pool sustain high bandwidth transmission at a central synapse. *Nature* **439**:983–987. DOI: https://doi.org/10.1038/nature04509, PMID: 16496000

Scheuss V, Neher E. 2001. Estimating synaptic parameters from mean, variance, and covariance in trains of synaptic responses. *Biophysical Journal* **81**:1970–1989. DOI: https://doi.org/10.1016/S0006-3495(01)75848-1, PMID: 11566771

Schmidt H, Brachtendorf S, Arendt O, Hallermann S, Ishiyama S, Bornschein G, Gall D, Schiffmann SN, Heckmann M, Eilers J. 2013. Nanodomain coupling at an excitatory cortical synapse. *Current Biology* **23**:244–249. DOI: https://doi.org/10.1016/j.cub.2012.12.007, PMID: 23273895

Schneggenburger R, Neher E. 2000. Intracellular calcium dependence of transmitter release rates at a fast central synapse. *Nature* **406**:889–893. DOI: https://doi.org/10.1038/35022702, PMID: 10972290

Sharma G, Vijayaraghavan S. 2003. Modulation of presynaptic store calcium induces release of glutamate and postsynaptic firing. *Neuron* **38**:929–939. DOI: https://doi.org/10.1016/S0896-6273(03)00322-2, PMID: 12818178

Shin OH, Lu J, Rhee JS, Tomchick DR, Pang ZP, Wojcik SM, Camacho-Perez M, Brose N, Machius M, Rizo J, Rosenmund C, Südhof TC. 2010. Munc13 C2B domain is an activity-dependent Ca2+ regulator of synaptic exocytosis. *Nature Structural & Molecular Biology* **17**:280–288. DOI: https://doi.org/10.1038/nsmb.1758, PMID: 20154707

Shu Y, Hasenstaub A, Duque A, Yu Y, McCormick DA. 2006. Modulation of intracortical synaptic potentials by presynaptic somatic membrane potential. *Nature* **441**:761–765. DOI: https://doi.org/10.1038/nature04720, PMID: 16625207

Silver RA, Momiyama A, Cull-Candy SG. 1998. Locus of frequency-dependent depression identified with multiple-probability fluctuation analysis at rat climbing fibre-Purkinje cell synapses. *The Journal of Physiology* **510**:881–902. DOI: https://doi.org/10.1111/j.1469-7793.1998.881bj.x, PMID: 9660900

Silver RA. 2003. Estimation of nonuniform quantal parameters with multiple-probability fluctuation analysis: theory, application and limitations. *Journal of Neuroscience Methods* **130**:127–141. DOI: https://doi.org/10.1016/j.jneumeth.2003.09.030, PMID: 14667542

Südhof TC. 2012. The presynaptic active zone. *Neuron* **75**:11–25. DOI: https://doi.org/10.1016/j.neuron.2012.06.012, PMID: 22794257

Tan YP, Llano I. 1999. Modulation by K^+ channels of action potential-evoked intracellular Ca^{2+} concentration rises in rat cerebellar basket cell axons. *The Journal of Physiology* **520**:65–78. DOI: https://doi.org/10.1111/j.1469-7793.1999.00065.x, PMID: 10517801

Taschenberger H, Scheuss V, Neher E. 2005. Release kinetics, quantal parameters and their modulation during short-term depression at a developing synapse in the rat CNS. *The Journal of Physiology* **568**:513–537. DOI: https://doi.org/10.1113/jphysiol.2005.093468, PMID: 16096340

Trigo FF, Chat M, Marty A. 2007. Enhancement of GABA release through endogenous activation of axonal GABA(A) receptors in juvenile cerebellum. *Journal of Neuroscience* **27**:12452–12463. DOI: https://doi.org/10.1523/JNEUROSCI.3413-07.2007, PMID: 18003823

Trigo FF, Sakaba T, Ogden D, Marty A. 2012. Readily releasable pool of synaptic vesicles measured at single synaptic contacts. *PNAS* **109**:18138–18143. DOI: https://doi.org/10.1073/pnas.1209798109, PMID: 23074252

Turecek R, Trussell LO. 2001. Presynaptic glycine receptors enhance transmitter release at a mammalian central synapse. *Nature* **411**:587–590. DOI: https://doi.org/10.1038/35079084, PMID: 11385573

Vere-Jones D. 1966. Simple stochastic models for the release of quanta of transmitter from a nerve terminal. *Australian Journal of Statistics* **8**:53–63. DOI: https://doi.org/10.1111/j.1467-842X.1966.tb00164.x

Wu LG, Saggau P. 1994. Pharmacological identification of two types of presynaptic voltage- dependent calcium channels at CA3-CA1 synapses of the Hippocampus. *The Journal of Neuroscience* **14**:5613–5622. PMID: 8083757

Zorrilla de San Martin J, Trigo FF, Kawaguchi SY. 2017. Axonal GABAA receptors depolarize presynaptic terminals and facilitate transmitter release in cerebellar Purkinje cells. *The Journal of Physiology* **595**:7477–7493. DOI: https://doi.org/10.1113/JP275369, PMID: 29072780

Zucker RS. 1973. Changes in the statistics of transmitter release during facilitation. *The Journal of Physiology* **229**:787–810. DOI: https://doi.org/10.1113/jphysiol.1973.sp010167, PMID: 4348351